



# 1 **Millennial-Scale Carbon Accumulation in Mediterranean Rhodolith**

## 2 **Deposits**

3 Silvia de Juan<sup>1</sup>, Ryan Smazal<sup>2</sup>, Claudio Lo Iacono<sup>3</sup>, Maria del Mar Gil<sup>1</sup>, Andrea Cabrito<sup>3</sup>, Andres Ospina-  
4 Alvarez<sup>1</sup>, Jorge Guillén<sup>3</sup>, Grace M. Cott<sup>2</sup>, Laia Illa-López<sup>1</sup>, Hilmar Hinz<sup>1</sup>, Francesc Maynou<sup>3</sup>

5 <sup>1</sup>Instituto Mediterráneo de Estudios Avanzados IMEDEA (UIB-CSIC), c. Miquel Marquès 21, 07190  
6 – Esporles (Spain)

7 <sup>2</sup>School of Biology and Environmental Science, University College Dublin, Dublin, Ireland

8 <sup>3</sup>Institut de Ciències del Mar (CSIC), Psg. Marítim de la Barceloneta 37-49, 08003-Barcelona (Spain)

9 *Correspondence to:* Silvia de Juan: [silvia.dejuan@csic.es](mailto:silvia.dejuan@csic.es)

10

11 **Abstract.** Rhodolith and maërl beds are globally relevant biogenic habitats whose long-term carbon  
12 storage capacity remains poorly quantified, particularly in the Mediterranean. To fill this gap, we  
13 investigated the formation, structure, and carbon content of a sediment deposit underlying a rhodolith  
14 bed in the Menorca Channel (Western Mediterranean). High-resolution seismo-acoustic profiling  
15 revealed a highly heterogeneous biogenic sedimentary deposit at ~60 m depth, with thickness ranging  
16 from a few centimeters to 3.7 m (mean = 0.95 m). Seven vibrocores extracted from the thickest sediment  
17 deposits were analyzed for grain size, carbonate content, bioclast composition, organic carbon, and  
18 radiocarbon age. Radiocarbon dating indicates that sediment accumulation began during the early  
19 Holocene (11,700–9,000 yr BP), when post-glacial sea-level rise transitioned the area from subaerial  
20 exposure to shallow-marine conditions. Early deposits were dominated by bivalves and dispersed  
21 coralline fragments. The establishment of modern sea level around 7,000–6,500 yr BP led to the  
22 development of dense rhodolith–maërl facies that persist today. Sediment accretion rates are low (median  
23 = 8.54 cm kyr<sup>-1</sup>), reflecting very low external sediment supply, and slow growth of coralline algae.  
24 Organic carbon content in the upper 50 cm, representing the most dynamic and recently deposited carbon  
25 pool, averaged 0.57% (± 0.22), with an estimated organic carbon stock of 32.04 (± 4.18) Mg C ha<sup>-1</sup>.  
26 These results show that Mediterranean rhodolith beds act as long-term organic carbon stores, forming  
27 spatially complex Holocene deposits whose contribution to carbon storage has been largely overlooked.

28 **Keywords**



29 Calcareous red algae; Sediment organic carbon; organic carbon sink; Holocene; Radiocarbon dating;  
30 Mediterranean Sea.

### 31 **Highlights**

- 32 • Seismo-acoustic mapping of a deep rhodolith deposits revealed highly variable thickness  
33 • Holocene sedimentation began 11,700–9,000 yr BP during post-glacial sea-level rise.  
34 • Dense rhodolith–maërl facies formed after sea-level stabilization ~7,000 yr BP.  
35 • Accretion rates are low (8.54 cm kyr<sup>-1</sup>), very low external sediment supply and slow algal growth.  
36 • Organic carbon averages 32.04 (± 4.18) Mg C ha<sup>-1</sup> in the upper 50 cm, evidencing long-term carbon  
37 storage.

38

39

40



## 41 1. INTRODUCTION

42 Marine habitats play a substantial role in the global carbon cycle by contributing to both organic and  
43 inorganic carbon storage. Coastal systems sequester atmospheric CO<sub>2</sub> through photosynthesis and the  
44 subsequent burial of sedimentary organic carbon, a process widely recognized as “blue carbon” (Barbier  
45 et al., 2011; Nellemann and Corcoran, 2009). Most knowledge of carbon burial in the coastal ocean  
46 comes from vegetated ecosystems such as mangroves, seagrass meadows and saltmarshes (Macreadie et  
47 al., 2019). In contrast, calcifying algal systems, such as rhodolith and maërl beds, remain comparatively  
48 understudied (Tuya et al., 2023). These systems are globally distributed and their deposits persist over  
49 millennia (Aguirre et al., 2016; Van der Heijden and Kamenos, 2015), suggesting a potential long-term  
50 carbon repository that has yet to be quantified at scale.

51 Rhodolith and maërl beds consist of free-living, non-geniculate calcareous red algae (Rhodophyta:  
52 Corallinophycidae) occurring as multi-specific assemblages (Cabrito et al., *under review*). These  
53 assemblages thrive in subtidal environments with coarse, mobile sediments under moderate  
54 hydrodynamic regimes that prevent burial while maintaining sufficient irradiance (Basso et al., 2017).  
55 They occur from shallow to mesophotic depths across tropical to polar regions (Riosmena-Rodríguez et  
56 al., 2017; Tuya et al., 2023). Despite their slow individual growth (~1 mm yr<sup>-1</sup>), rhodolith accumulations  
57 can reach several meters in thickness over hundreds to thousands of years, with living rhodoliths limited  
58 to the upper few centimeters, above deposits of fragmented coralline algae and skeletal remains of  
59 bryozoans, molluscs, and echinoderms (Betzler et al., 2011; Fornós and Ahr, 1997).

60 Rhodolith and maërl beds have the capacity to store carbon through the long-term accumulation of thick,  
61 carbonate-rich sediments that can remain stable over centuries to millennia (Mao et al., 2020). In contrast  
62 to other well-known blue carbon habitats, their contribution to carbon storage is not driven by short-term  
63 biological processes but result from the long-term accumulation of biogenic deposits and the trapping  
64 and retention of organic carbon supplied from external sources (Mao et al., 2020; Schubert et al., 2024).  
65 However, empirical data on sediment organic carbon content, depth distribution, sediment dynamics and  
66 accretion history remain limited, particularly in Mediterranean rhodolith beds. Quantifying these  
67 components is essential to evaluate the role of this ecosystem as long-term carbon reservoirs.

68 Large rhodolith and maërl beds are present on modern and ancient carbonate shelves around the world  
69 (Riosmena-Rodríguez et al., 2017), including the world’s largest bed on the Brazilian continental shelf  
70 (21 000 km<sup>2</sup>, Amado-Filho et al., 2012). The Mediterranean hosts the second-largest bed described to  
71 date, covering approximately 470 km<sup>2</sup> in the Menorca Channel, western Mediterranean (Tabone et al.,



72 2024). Its development has been facilitated by the clear waters and low sediment input that characterize  
73 Mediterranean islands, allowing rhodolith beds to extend down to 90 m depth (Joher et al., 2016).  
74 However, despite their ecological importance, the functioning and carbon dynamics of Mediterranean  
75 rhodolith beds remain poorly resolved, particularly regarding organic carbon accumulation, small-scale  
76 spatial heterogeneity and the long-term evolution of these deposits.

77 These biogenic habitats are highly vulnerable to disturbance due to their slow growth and limited  
78 recovery capacity, and are threatened by bottom-contact fishing gears, elevated suspended sediments,  
79 and the cumulative effects of ocean warming and acidification under climate change (Trégarot et al.,  
80 2024; Tuya et al., 2023). Although Mediterranean rhodolith beds are protected under EU Regulation  
81 1997/2006, the EU Habitats Directive, and the UNEP/MAP Action Plan (2008), conservation remains  
82 limited due to insufficient spatial coverage and ecological data. Strengthening the scientific basis for  
83 management aligns with European priorities linking biodiversity conservation, climate-change  
84 mitigation, and ecosystem restoration. In this context, improving knowledge of the organic carbon  
85 storage capacity of rhodolith beds is essential to help quantify their role in the global carbon cycle,  
86 particularly given their broad geographic distribution (de Macêdo Carneiro et al., 2021; Schubert et al.,  
87 2024).

88 This study quantifies the role of Mediterranean rhodolith beds as long-term organic carbon reservoirs by  
89 analyzing sedimentary organic carbon deposition since the early Holocene post-glacial sea-level rise,  
90 along with geomorphological and sedimentary characterization of a well-preserved deposit in the  
91 Menorca Channel (western Mediterranean). The Menorca Channel is a low-energy temperate carbonate  
92 shelf where rhodolith sediments have accumulated since the early Holocene, providing a unique archive  
93 to examine carbon storage over millennial timescales. Using high-resolution seismo-acoustic data and  
94 sediment cores and radiocarbon dating, we estimate the vertical distribution of organic carbon and  
95 reconstruct the depositional history through in relation with the last glacio-eustatic oscillation. We test  
96 the hypothesis that this rhodolith bed represents a persistent Holocene carbon store shaped by local  
97 environmental conditions and long-term sea-level changes, with implications for regional blue carbon  
98 assessments.

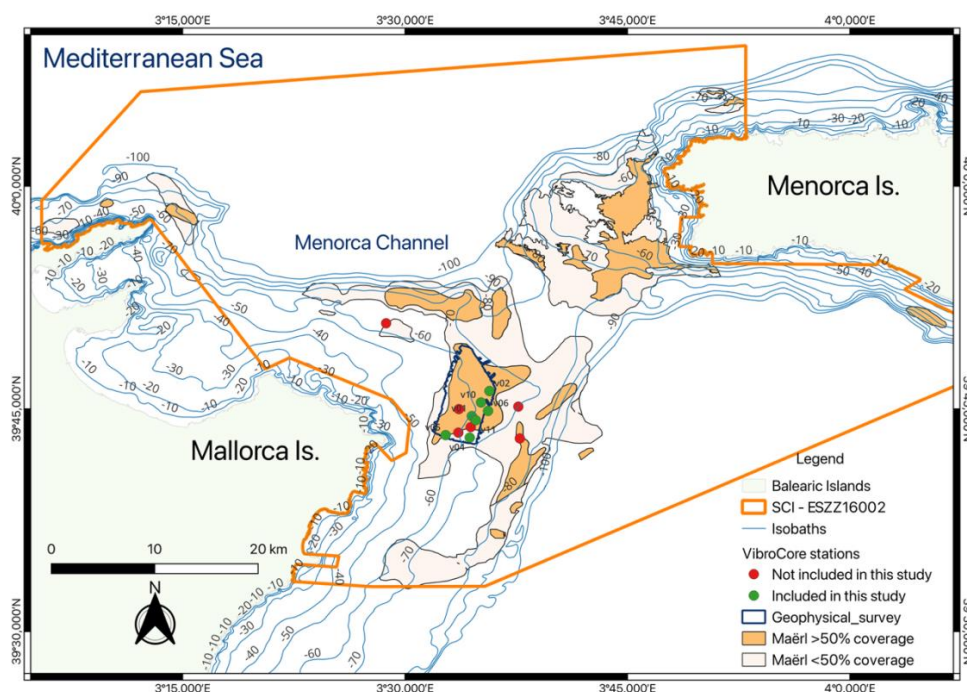
## 99 **2. MATERIAL AND METHODS**

### 100 **2.1. Study area**

101 The Balearic continental shelf is a temperate, low-energy oligotrophic system dominated by carbonate-  
102 producing habitats, including *Posidonia oceanica* meadows, coralligenous communities, and extensive



103 rhodolith–maërl beds (Betzler et al., 2011; Canals and Ballesteros, 1997). Our study focuses on the  
104 Menorca Channel, a shallow carbonate platform (~100 m max depth) between Mallorca and Menorca,  
105 where post-glacial neritic carbonates have accumulated since the early Holocene (Alonso et al., 1988;  
106 Betzler et al., 2011). Rhodolith and maërl beds occur between 45–80 m depth on the platform (Fig. 1),  
107 interspersed with detrital sands and other macroalgae (*Laminaria rodriguezii*, *Osmundaria*  
108 *volubilis*, *Peyssonnelia rosa-marina*) (de Juan et al., 2023). Habitat preservation has been favored by a  
109 historical trawling exclusion zone surrounding submarine cables and, more recently, by the 2016  
110 designation of the Menorca Channel as a Natura 2000 Site of Community Importance (SCI ESZZ16002).  
111 We focused on a 43.6 km<sup>2</sup> area where rhodolith and maërl cover exceeds 50%, based on high-resolution  
112 mapping from the INDEMARES project (Moranta et al., 2014) and our own video surveys (Cabrito et  
113 al., 2024b). Within this area, we conducted high-resolution seismo-acoustic profiling to determine the  
114 thickness of bioclastic sediments above the acoustic basement and to identify suitable sites for recovering  
115 ≥1-m sediment cores. Potential sites were inspected with a remotely operated vehicle (ROV) to confirm  
116 rhodolith–maërl dominance, and full coverage was verified at all core locations.



117

118 **Figure 1.** Study area in the Menorca Channel, located between Mallorca and Menorca islands in the western Mediterranean  
119 Sea. The map shows the area covered by the geophysical survey (dark blue polygon) and the location of VibroCore stations  
120 included (green dots) and not included (red dots) in this study. Rhodolith are represented in light and dark orange, indicating  
121 areas with 10-50% and >50% coverage, respectively. The Site of Community Importance (SCI ESZZ16002) is delineated by  
122 the dark orange boundary. Isobaths (in metres) are shown as blue contour lines. Source: modified from project  
123 INDEMARES (Moranta et al., 2014).



124

## 125 2.2. Geophysical map

126 In May 2022, we acquired 56 high-resolution seismo-acoustic profiles in the study area (Fig. 1) during a  
 127 research cruise aboard R/V *SOCIB* and using an INNOMAR Medium-100 non-linear parametric  
 128 echosounder coupled with an INS SBG Navisight Ekinox and GNSS AtlasLink for positioning. Sound-  
 129 speed and turbidity corrections were obtained with a Valeport SWIFT. The system emits two primary  
 130 frequencies around 100 kHz, producing a secondary frequency of 5–12 kHz, with a pulse repetition rate  
 131 of up to 30 s<sup>-1</sup> and a beam width of ±1.8°. Non-linear parametric echosounders provide narrow, low-  
 132 frequency beams with small footprints, enabling high-resolution imaging of shallow sediment deposits  
 133 and precise localization of core-sampling targets (Lo Iacono et al., 2008).

134 Profiles were spaced 200 m apart, oriented NNE–SSW in the southern sector and NW–SE in the northern  
 135 sector, intersected by perpendicular transversal profiles every 500–2000 m (supplementary material 1).  
 136 Penetration depth averaged 0.8–1.0 m and reached a maximum of 3.7 m, maintaining high horizontal and  
 137 vertical metric to sub-metric resolution due to the small pulse size. Seismo-acoustic data were interpreted  
 138 using INNOMAR-ISE 2.9 to pick stratigraphic horizons and estimate thickness of the bioclastic deposit.  
 139 Geo-referencing and isopach mapping were conducted with Global Mapper and ArcGIS.

## 140 2.3. Sediment core sampling

141 In May 2023, sediment cores were collected at 60–80 m depth during a research cruise aboard  
 142 R/V *Sarmiento de Gamboa*. Cores' positions were selected based on geo-acoustic evidence of maximum  
 143 sediment thickness within the survey polygon (Fig. 2). A vibrocorer (ASTHER I, GEOMY TSA S.A.)  
 144 operating at 136 kN centrifugal force at 3 m recovered 12 PVC-lined cores (9 cm diameter, 1.4–2.8 m  
 145 length; Table 1). Each core was sectioned into ≤1 m segments and stored at –20 °C for laboratory  
 146 analyses. Of the 12 cores, 7 were retained for this study (Fig. 1).

147 **Table 1** – Characteristics of the seven vibrocores obtained in the Menorca Channel (Western Mediterranean) selected for  
 148 this study. Description of biocenoses based on knowledge from our own video observations (projects MaCoBioS;  
 149 MARBEFES) and previous projects (INDEMARES).

Vibrocore ID	Longitude	Latitude	Sea bottom Depth (m)	core length (m)	analyses	biocenose
V1	3.5750	39.7419	61.91	1.60	+ * #	rhodoliths >75%, with Peyssonnelia and Osmundaria
V2	3.5949	39.7700	66.22	1.40	+ * \$ #	rhodoliths >75%, with Laminaria
V4	3.5727	39.7177	66.08	1.80	+ * \$ #	rhodoliths >60%, with Osmundaria
V5	3.5456	39.7205	60.01	2.80	+ * #	rhodoliths >60%, with Osmundaria
V6	3.5933	39.7477	64.52	1.90	+ * \$ #	rhodoliths >60%, with Laminaria



<b>V10</b>	3.5854	39.7572	63.28	1.45	+ * #	rhodoliths >90%, with Peyssonnelia
<b>V11</b>	3.5794	39.7525	63.93	1.75	+ * \$ #	rhodoliths >75%, with Peyssonnelia

150 + Lithology and clasts composition; \* Granulometry and carbonates; \$ Radiocarbon dating; # Organic carbon

151

## 152 **Sediment core opening and visual description**

153 Each 1-m core section was cut longitudinally for analysis. All cores were visually inspected to describe  
 154 sediment composition, and subsamples were collected for grain size, radiocarbon dating, bioclast  
 155 identification, and organic carbon content analyses.

## 156 **Grain size and carbonate contents**

157 The cores were sampled at 5 cm intervals for grain-size and carbonate-content analyses. Grain-size  
 158 distributions were measured using a HORIBA LA-950V2 laser diffraction analyser after disaggregating  
 159 and removing the biogenic fraction (10% H<sub>2</sub>O<sub>2</sub>), and ultrasonic dispersion; the >2 mm fraction was  
 160 quantified by sieving. We calculated the weight percentages of clay, silt, sand, and gravel, as well as  
 161 mean grain size ( $\phi$ ), sorting ( $\sigma$ ), skewness (Sk), and kurtosis (kG). Carbonate content was determined  
 162 from the CO<sub>2</sub> volume displaced by a sample of sediment treated with 20% HCl, calibrated against a 100%  
 163 CaCO<sub>3</sub> standard.

## 164 **Radiocarbon dating**

165 Between two and three bioclasts (rhodoliths or bivalve shells) from different depths in four cores (Table  
 166 1) were radiocarbon-dated by Beta Analytic (Miami, USA). Dates were calibrated with BetaCal 5.0, with  
 167 HPD method “MARINE20” and corrected for the local marine reservoir effect ( $\Delta R = -112 \pm 99$ ).  
 168 Sediment accretion rates (cm kyr<sup>-1</sup>) were calculated by dividing the thickness of sediment between  
 169 successive dated horizons along the core (kyr), taking the top most horizon as 0 yr BP.

## 170 **Taxonomic identification of bioclasts**

171 Sediment was examined under a binocular microscope at ~50 cm intervals for fauna identification.  
 172 Subsamples (10–20 g) were air-dried (48 h) and sieved through 0.5 and 1 mm meshes. Between 200 and  
 173 300 clasts from the >0.5–1 mm and >1 mm fractions were inspected and assigned to major taxonomic  
 174 groups (Bivalves, Gastropods, Bryozoans, Echinoids, Foraminiferans, and free-living coralline algae).  
 175 Rhodoliths were classified into two morphotypes following (Basso, 1998; Basso et al., 2012): non-  
 176 branched rhodoliths (including “boxwork” and “praline” forms; 1–5 cm) and branched maërl fragments  
 177 (0.5–2 cm) (see also Jardim et al., 2025; Teichert, 2024).



## 178 **2.4. Organic Carbon Content**

179 From each core, sediment samples (~21 ml) were collected using a syringe every 10 cm within the upper  
180 50 cm, as this layer is expected to contain the highest and more dynamic carbon pool, which has not yet  
181 undergone long-term diagenesis (Middelburg, 2018). To minimize decomposition of organic matter and  
182 microbial growth, samples were kept cold (4 °C) during 24-48 for later processing. In the laboratory,  
183 samples were weighed, freeze-dried (lyophilized) for 48-72 hours, and weighed again to determine their  
184 moisture content percentage. Finally, the samples were finely ground in an agate ball mill.

185 The processed samples were subsequently sent to University College Dublin to be sub-sampled for  
186 further analysis. From each 10 cm layer, ~2.0 g ( $\pm 0.6$  g) of homogenized sediment was subsampled for  
187 organic carbon analysis. A sub-set of the homogenized sample was then shipped to the University of  
188 Waterloo (Canada) for carbon and nitrogen analysis. The samples were analysed using an ECS 4010  
189 Elemental Analyzer (NC Technologies, Italy) coupled to a Delta Plus XL (Thermo-Finnegan, Germany)  
190 continuous flow isotopic mass spectrometer (CRFIRMS). Samples were acid washed according to the  
191 University of Waterloo Environmental Isotope Laboratory procedures in order to remove inorganic  
192 carbon and obtain organic carbon measurements. High effervescence during acid treatment indicated a  
193 substantial carbonate fraction, resulting in a marked mass loss. The %C and %N was measured in bulk,  
194 analyzed against known certified elemental standard materials. Analytical control measures were based  
195 on the detection of major carbon (C) and nitrogen (N) peaks to ensure data consistency and calibration  
196 accuracy.

## 197 **2.5. Data analysis**

198 To evaluate whether sediment characteristics control the density of retained organic carbon, variation in  
199 organic carbon density ( $\text{g}/\text{cm}^3$ ) was analysed in relation to sediment characteristics using linear mixed-  
200 effects models to account for the hierarchical structure of the sampling design, with multiple depth  
201 subsamples collected within each sediment core. Because organic carbon density values were positive  
202 and right-skewed, the response was log-transformed ( $\log[\text{CarDens}]$ ) and modelled assuming Gaussian  
203 errors. Core identity was included as a random intercept to accommodate non-independence among  
204 subsamples from the same core.

205 The following sediment characteristics that were explored as candidate fixed effects were: standardized  
206 sediment depth (cm), median grain size ( $d_{50}$ ;  $\mu\text{m}$ ), carbonate content (%), biogenic gravel content (%),  
207 and sediment type (categorical). Owing to strong collinearity between  $d_{50}$  and the sand/silt fractions ( $|r|$   
208  $\approx 0.90$ – $0.96$ ), grain-size fractions were not included in models containing  $d_{50}$ . Potential within-core



209 residual dependence across depth was evaluated by fitting models with an AR(1) correlation structure  
210 along depth within each core. In addition, a random-slope formulation allowing core-specific depth  
211 trends was tested using a diagonal random-effects structure (random intercept and depth slope by core,  
212 with intercept–slope covariance constrained to zero). Models were compared using AICc, with maximum  
213 likelihood estimation used for model selection and the best-supported model refitted by restricted  
214 maximum likelihood for final parameter estimation. The intraclass correlation coefficient (ICC) was  
215 calculated from variance components to quantify the proportion of variance attributable to differences  
216 among cores. All analyses were conducted in R v4.4.2.

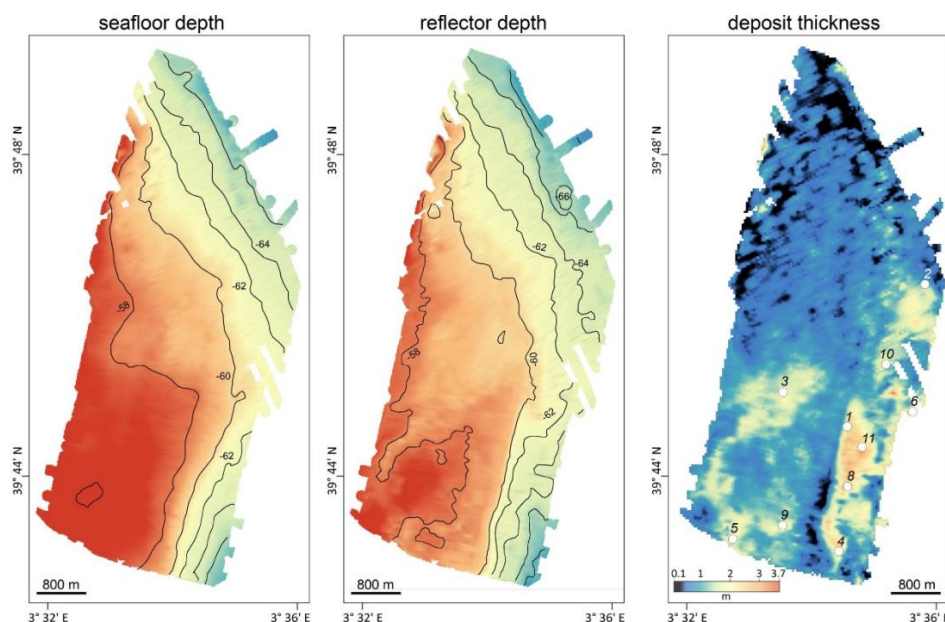
### 217 **3. RESULTS**

#### 218 **3.1. Seismoacoustic records**

219 The surveyed area ranges from 57 to 68 m depth and exhibits generally smooth bathymetry, with an  
220 average slope of  $0.2^\circ$ . The western sector is relatively flat, gradually deepening from 57 to 60 m, while  
221 the southeast and northeast show narrow bathymetric edges with steeper slopes reaching 68 m (Fig. 2).

222 Geo-acoustic profiles allowed detailed mapping of the 3D architecture of the bioclastic deposit. Sediment  
223 thickness was highly heterogeneous at small scales, ranging from nearly 0 to several meters over spatial  
224 extents of hundreds of meters or less (Fig. 2, right panel; supplementary material 1). Average thickness  
225 was 0.95 m, with a maximum of 3.7 m. Thinner deposits occurred in the northern sector (down to 10 cm),  
226 whereas thicker accumulations were found in the southern and eastern sectors, including a  $2 \text{ km} \times 1 \text{ km}$   
227 patch reaching 3.7 m at its depocenter.

228 Cores were collected at locations of maximum sediment accumulation. Of the seven cores retained for  
229 this study, V1, V2, and V10 reached the bedrock horizon; V4, V6, and V11 fell short by 0.5–1.1 m; and  
230 V5 slightly penetrated the bedrock ( $\sim 1 \text{ m}$ ) (Figs. 2 and 3; supplementary material 1).



231  
232  
233  
234  
235

**Figure 2.** Results of the high-resolution profiling in the rhodolith deposit. Left panel: bathymetry, central panel: reflector depth, right panel: deposit thickness. Refer to position of geophysical survey in Fig. 1.

### 236 **3.2. Sediment characteristics**

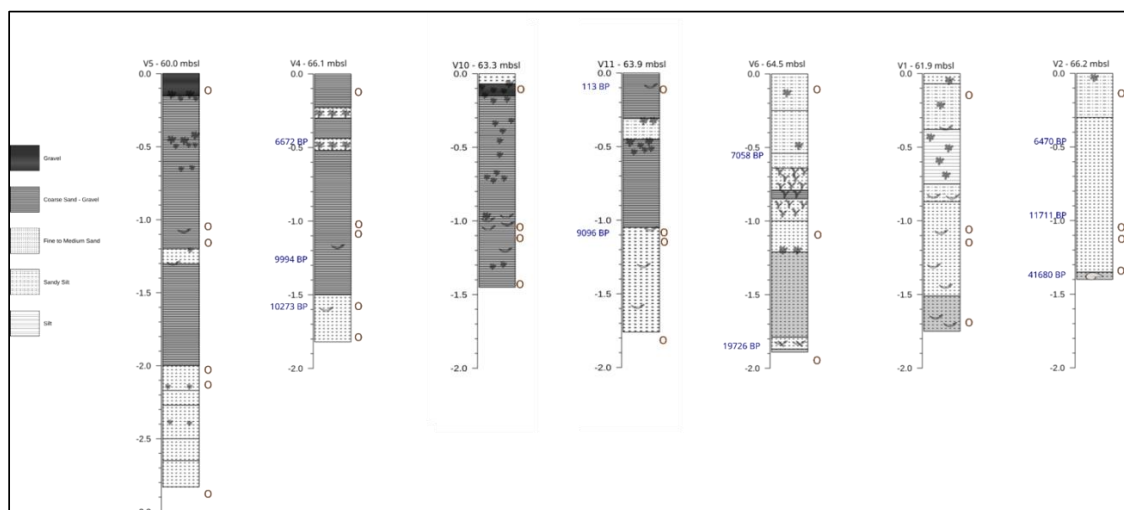
237 Visual inspection of the cores revealed a relatively uniform composition, dominated by fine to coarse  
238 bioclastic sand with occasional horizons of gravel or silt (Fig. 3; supplementary material 2). Grain-size  
239 analysis confirmed sand as the dominant fraction (>50%), with fines occasionally higher in certain  
240 horizons (e.g., V1: 40–90 cm; V2: 30–60 cm; V4: 25–65 cm; V6: 25–60 cm; V11: 35–65cm), but never  
241 exceeding sand content. Gravel was always <25%, with the exception of V5: 40–50 cm, 50% gravel.  
242 Carbonate contents were consistently  $\geq 90\%$  along the cores.

243 Sediment composition was primarily carbonate bioclasts (75%) and, to a lesser extent, carbonate  
244 lithoclasts (8%), with variable contributions from siliciclastic grains. Stereomicroscope analysis allowed  
245 identification of 65% of clasts, mainly unattached coralline red algae (26%, branched and non-branched),  
246 bivalve fragments (22%), gastropods (13%), echinoid remains (4%), foraminifera (4%), and bryozoans  
247 (3%). Minor groups included serpulids, ostracods, and polyplacophorans. Siliciclastic grains (17%) were  
248 grey or white lithoclasts, distinguished by texture and lack of reaction to dilute HCl.

249 Coralline algae fragments occurred throughout the cores, whereas well-formed rhodoliths were confined  
250 to the upper ~60 cm (except V2), occurring either scattered or densely packed, particularly in V4, V5,



251 and V11 (Fig. 3). Three cores (V1, V2, V6) terminated on cemented substrate, including bivalve-rich  
 252 hardgrounds or reworked lithoclasts.



253  
 254 **Figure 3.** Stratigraphic columns showing the lithological composition of the sediment and radiocarbon dates (in blue).  
 255 Circles: sampling for faunistic identification: o Clasts (only clasts > 5 cm are represented): non-branched rhodolith: \*  
 256 branched rhodolith: Y entire bivalve shell: broken bivalve shell: rock fragment:

### 258 3.2.1. Radiocarbon Dating

259 Radiocarbon dating of rhodoliths and bivalve shells from four cores (Table 2) yielded ten age estimates.  
 260 Two basal ages (41,680 yr BP in V2 and 19,726 yr BP in V6) indicate reworked pre-Holocene material  
 261 from periods when the area was in an emerged sub-aerial setting. The next four oldest dates, between  
 262 11,711 and 9,096 yr BP, correspond to the end of Younger Dryas (11,711 yr BP) and the subsequent rapid  
 263 sea-level rise (until 9,000 yr BP), indicating that the area was a shallow marine environment (<20 m  
 264 depth) dominated by bivalves and dispersed branched rhodoliths. Some lithoclasts within these horizons  
 265 indicate continental input consistent with shallow-water conditions.

266 **Table 2.** Radiocarbon dates (<sup>14</sup>C) for carbonate bioclasts obtained from the testing laboratory of Beta Analytic (Miami, FL,  
 267 US), recalibrated with BetaCal 5.0 and corrected for the local marine reservoir effect (-112 ± 99).  
 268

Core	Depth (cm)	Radiocarbon Date BP	Calibrated Probability Data (2 sigma)	Calibrated years BP
V2	136	37934 ± 875	41146-38315 BC 100%	41680.5
V2	97	10490 ± 30	10151-9371 BC 95.4%	11711
V2	47	6110 ± 30	4778-4261 BC 95.4%	6470
V4	160.5	9460 ± 30	8640-8006 BC 95.4%	10273
V4	117.5	9270 ± 30	8372-7716 BC 95.4%	9994
V4	46	6300 ± 30	5000-4444 BC 95.4%	6672
V6	183	28067 ± 392	30634-4918 BC 100%	19726

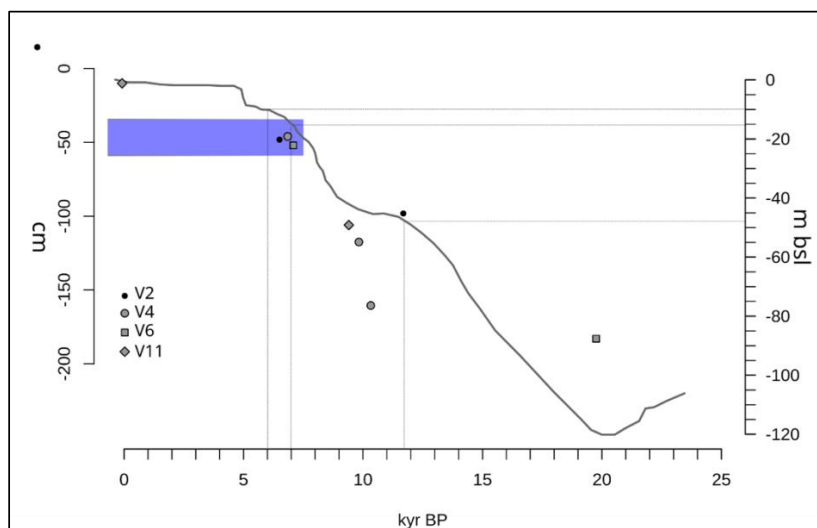


<b>V6</b>	52	6552 ± 81	5298-4918 BC 100%	7058
<b>V11</b>	106	8530 ± 30	7455-6837 BC 95.4%	9096
<b>V11</b>	10	340 ± 30	1724-1950 BD 95.4%	113

269

270 Three younger ages, between 7,058 and 6,470 yr BP (47–52 cm depth in V2, V4, and V6), correspond to  
 271 a period when the Menorca Channel was ~10–15 m below present sea level, during which well-formed,  
 272 densely packed rhodoliths accumulated (Fig. 3). During this interval, continental inputs diminished,  
 273 maërl became abundant, and rhodolith beds consolidated, as exemplified by V4 (~50 cm, 6,672 yr BP).  
 274 Scattered rhodolith fragments occasionally occur at greater depths, but none are found in strata older than  
 275 9,096 yr BP, highlighting the onset of persistent rhodolith accumulation after postglacial transgression.

276 Based on these dates, sediment accretion rates range from 6.9 to 21.5 cm kyr<sup>-1</sup>, with a median of 8.54  
 277 cm kyr<sup>-1</sup> (Fig. 4).



278

279

280 **Figure 4.** Age-depth plot for the dated cores (excluding one sample that yielded a date > 40 ky BP) from the rhodolith  
 281 deposit of the Menorca channel. Sea-level height (m) relative to present day based on the average model from (Bianchi et  
 282 al., 2012), largely based on results from (Lambeck and Bard, 2000). Relevant dates for this deposit (end of Younger Dryas at  
 283 11700 yr BP and period of sea level stabilization between 7000 and 6000 yr BP) are marked along the x-axis and the  
 284 corresponding depth below current sea level on the right y-axis. Blue stripe between 35 and 60 cm core depth shows the  
 285 onset of horizons with high abundance of rhodoliths.

286

### 287 3.3. Organic Carbon content

288 The average organic carbon content in the first 50 cm of sediment across all cores was 0.57% (± 0.22)  
 289 (Table 3). This value remained relatively homogeneous with depth (supplementary table 1). Using these  
 290 measurements, organic carbon stocks were determined for each core. Over the first 30 cm, we estimate



291 an average across all the cores of  $19.41 (\pm 4.42) \text{ Mg C ha}^{-1}$ . Over the full 50 cm, we estimate an organic  
292 carbon stock of  $32 (\pm 4.18) \text{ Mg C ha}^{-1}$  across all coring sites (Table 3). Considering a median sediment  
293 accretion rate of  $8.54 \text{ cm kyr}^{-1}$ , annual organic carbon accumulation is estimated at  $0.546 \text{ g C m}^{-2} \text{ yr}^{-1}$ .

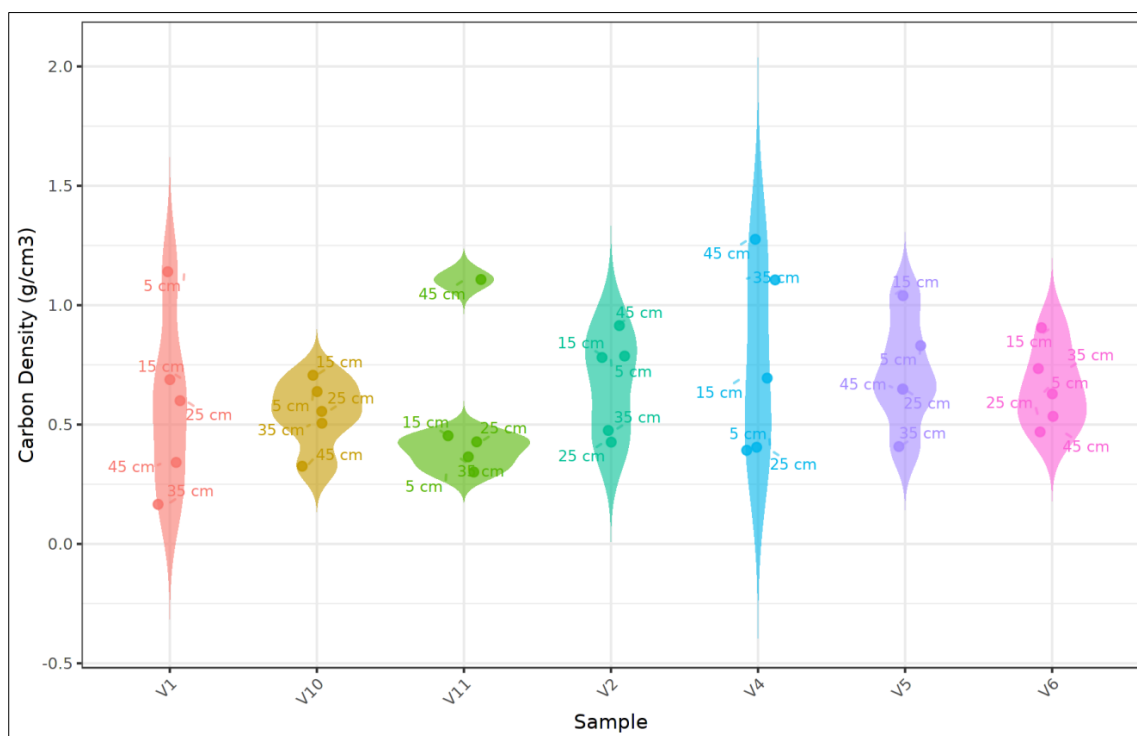
294 The molar C/N ratios were used to assess the origin and degree of degradation of the organic matter. The  
295 average C/N ratio across all samples was  $10.71 (+/-3.19)$ , with the highest value being  $18.51$  (V11) and  
296 the lowest value being  $7.71$  (V4) indicating predominantly marine sources.

297 **Table 3.** Summary table showing the average organic carbon density, the stock over the top 30 cm and the total length of the  
298 core.

Core	Avg C Density ( $\text{kg C m}^{-3}$ )	Carbon Stock Top 30 cm ( $\text{Mg C ha}^{-1}$ )	Carbon Stock 50 cm ( $\text{Mg C ha}^{-1}$ )
V1	5.87	24.28	29.36
V2	6.77	19.94	33.84
V4	7.75	14.92	38.74
V5	7.15	25.19	35.75
V6	6.54	20.68	32.72
V10	5.46	18.99	27.31
V11	5.031	11.82	26.54
All Cores	6.41	19.41	32.04

305

306 Mixed-effects modelling indicated that organic carbon density in the upper 50 cm was primarily  
307 explained by carbonate content and grain size ( $d_{50}$ ), with a weaker contribution from biogenic gravel  
308 content, while depth showed no consistent effect. Alternative model structures, including sediment type,  
309 random slopes for depth, and AR(1) correlation across depth, did not improve model fit and were not  
310 retained (see supplementary table 2). In the final model,  $d_{50}$  was positively associated with organic  
311 carbon density ( $\beta = 0.177$ ,  $p = 0.0046$ ) and carbonate was negatively associated with organic carbon  
312 density ( $\beta = -0.306$ ,  $p < 0.001$ ), whereas biogenic gravel showed a weaker positive association ( $\beta =$   
313  $0.098$ ,  $p = 0.0688$ ) and depth was not significant ( $p = 0.577$ ). Approximately 42% of the variability in  
314 organic carbon density was attributable to differences among cores, with the remaining variance  
315 occurring within cores and as unexplained residual variability (Fig. 5).



316

317 **Figure 5.** Organic carbon density in the sediments ( $\text{g}/\text{cm}^3$ ) of the first 50 cm of corers.

318

#### 319 4. DISCUSSION

320 The Holocene sedimentary deposit underlying the present-day rhodolith bed in the Menorca Channel is  
 321 relatively thin and heterogeneous. It overlies an erosional unconformity formed during postglacial sea-  
 322 level rise and likely includes reworked Miocene–Pliocene deposits (Guillén, 1987). Across the surveyed  
 323 area (57–68 m depth range), bathymetry is generally smooth, with a gentle average slope ( $\sim 0.2^\circ$ ): the  
 324 western sector is relatively flat, while the southeast and northeast margins are marked by narrow  
 325 bathymetric edges and locally steeper slopes. Sediment thickness varies markedly, from  $\sim 10$  cm in the  
 326 northern sector to up to 3.7 m in the south and east, with a mean value of 0.95 m. This spatial variability  
 327 reflects the combined influence of variable local scale paleo-topography and hydrodynamics, as observed  
 328 in other temperate carbonate continental shelves (Betzler et al., 2011; Fornós and Ahr, 1997). Mapping  
 329 sediment thickness was essential to recover cores with sufficient depth to reconstruct the millennial-scale  
 330 depositional history of this ecosystem.



331 Radiocarbon data indicate that rhodolith assemblages in the Menorca Channel pre-date the large maërl  
332 deposits of western France (5,860–5,300 yr BP, Ehrhold et al., 2021) but are younger than the oldest  
333 known rhodoliths from the Gulf of Mexico (13,886 yr BP, Olmstead and Andrus, 2024). Early Holocene  
334 deposits, formed at the end of the Younger Dryas and during rapid postglacial sea-level rise, reflect a  
335 shallow-marine environment dominated by bivalves and dispersed branched rhodoliths. Well-formed  
336 rhodoliths only became established in the upper ~60 cm of sediment, once deeper and more stable marine  
337 conditions developed around 7,000–6,000 yr BP (Lambeck, 1995), when sea-level lowered down its rise  
338 almost reaching its actual level . This interval marks a clear transition to dense rhodolith beds,  
339 characterized by large, tightly packed rhodoliths. The expansion and persistence of rhodoliths were likely  
340 promoted by moderate hydrodynamics, reduced terrigenous input, and mesophotic depths that limit  
341 competitive pressure (Aguirre et al., 2012; Basso et al., 2017). These conditions underpin the long-term  
342 stability of these habitats in the Menorca Channel.

343 Present-day seafloor patterns in the Menorca Channel are characterized by patches of rhodoliths  
344 occurring at high densities (50–100%), ranging in size from ~10 m<sup>2</sup> to over 100 m<sup>2</sup>, and predominantly  
345 composed of branched forms (Cabrito et al., 2024a, b), resembling the upper layers of the sediment cores.  
346 Despite being collected at similar depths and within short distances (600–1,700 m), the cores show  
347 marked spatial sedimentological variability, likely reflecting the irregularity of the basal erosive surface.  
348 Spatial differences in sediment thickness and repeated phases of erosion and deposition have shaped the  
349 present bioclastic landscape and supported the long-term development of rhodolith-rich habitats. This  
350 persistence through time underscores the capacity of these systems to maintain structural complexity  
351 over millennial timescales and act as organic carbon reservoirs, with important implications for their  
352 conservation and management. Similar patchy and heterogeneous distributions have been reported in  
353 other deep Mediterranean rhodolith beds (Bracchi et al., 2022; Rendina et al., 2020; Tabone et al., 2024).

354 The sediments throughout the cores are highly carbonate-rich ( $\geq 90\%$ ) and dominated by bioclastic  
355 material (~75%), including coralline algal fragments (branched and non-branched), bivalves, gastropods,  
356 echinoids, foraminifera, and bryozoans. Organic carbon in the upper 50 cm averages 0.57% and is also  
357 relatively uniform across the sampled section. In contrast, sediment thickness is highly heterogeneous at  
358 small spatial scales, ranging from a few centimeters in the northern sector to up to 3.7 m in the south and  
359 east, implying spatial variability in potential carbon storage. Reflecting these patterns, mixed-effects  
360 modelling evidenced that depth within the sediment cores had no detectable effect, and approximately  
361 42% of the variability in organic carbon density was attributable to differences among cores, indicating



362 pronounced small-scale patchiness in carbon accumulation across the rhodolith bed. The absence of depth  
363 trends could suggest relatively uniform near-surface mixing and burial, maintained by bioturbation and  
364 hydrodynamic reworking, while moderate among-core heterogeneity might reflect local patchiness in  
365 rhodolith morphology and accumulation; however, the limited number of cores prevents strong  
366 conclusions. The organic carbon density was partially explained by sediment composition, with higher  
367 carbonate content associated with lower carbon density, and coarser grain size ( $d_{50}$ ) showing a positive  
368 effect, consistent with dilution in carbonate-rich sediments and a textural control on carbon storage  
369 (Howard et al., 2018; Keil et al., 1994).

370 The relatively uniform organic carbon content in the upper 50 cm suggests minimal degradation over  
371  $\sim 6,000$  years, coinciding with the stabilization of the sea level. This stability likely promoted the  
372 development of well-formed rhodolith habitats, facilitating organic carbon capture and retention. Future  
373 work should examine deeper sediment layers ( $>50$  cm) to assess carbon preservation at greater depths.  
374 We estimate an organic carbon stock of approximately  $32.04 \text{ Mg C ha}^{-1}$  within the upper 50 cm of  
375 sediment across all the cores, with an average of  $19.41 (\pm 4.42) \text{ Mg C ha}^{-1}$  over the top 30 cm.  
376 Considering a median sediment accretion rate of  $8.54 \text{ cm kyr}^{-1}$ , annual organic carbon accumulation is  
377 estimated at  $\sim 0.546 \text{ g C m}^{-2} \text{ yr}^{-1}$ . These values exceed previous estimates reported for coralline algal  
378 beds in temperate coastal environments. For example, Mao et al. (2020) reported average organic carbon  
379 stocks of  $7.23 \pm 1.30 \text{ Mg C ha}^{-1}$  within the upper 25 cm and  $12.28 \pm 1.98 \text{ Mg C ha}^{-1}$  across the full depth  
380 of carbonate deposits ( $\sim 80$  cm) in Scottish coastal rhodolith beds. The substantially higher carbon stocks  
381 observed in the Menorca deposit likely reflect its long-term depositional stability and slow sediment  
382 turnover. Rather than acting as a rapid carbon sink, this system functions as a millennial-scale carbon  
383 reservoir, preserving organic matter within a very slowly forming carbonate matrix and highlighting its  
384 ecological and climatic importance despite low annual productivity.

385 Given their extremely slow sediment accretion rates, these organic carbon deposits are highly vulnerable  
386 to physical disturbance, particularly from bottom-contact fishing such as trawling and dredging (Trégarot  
387 et al., 2024). These activities can fragment nodules, bury living rhodoliths, and alter the structure and  
388 compaction of the sediment, with impacts that persist over timescales far longer than ecosystem  
389 management schemes (Cabanellas-Reboredo et al., 2018; de Juan et al., 2013; Tauran et al., 2020). The  
390 upper few centimeters of the deposit can be disrupted by a single trawling passage, not only halting  
391 carbon sequestration but potentially remobilizing organic carbon that accumulated over thousands of  
392 years (Bernard et al., 2019). In the Mediterranean, many rhodolith beds remain exposed to such pressures,



393 as they alternate with soft-sediment habitats that overlap with commercial trawling grounds (Illa-López  
394 et al., 2023; de Juan et al., 2013). In contrast, the Menorca Channel deposit has been largely protected  
395 from trawling due to the historical presence of submarine communication cables and its designation as a  
396 trawl-banned area since 2016. Evidence from this untrawled site suggests relatively uniform carbon  
397 preservation and burial under natural, undisturbed conditions. The evidence of organic carbon storage  
398 potential highlights the need for future research into rhodolith beds. In particular, this would include  
399 assessing whether organic carbon stored in sediments, as opposed to carbon produced via rhodolith  
400 calcification, is sequestered at rates that balanced or exceed calcification-related carbon release. This  
401 highlights the critical role of protection in maintaining the long-term carbon storage and ecological  
402 integrity of rhodolith habitats.

## 403 **Conclusions**

404 Rhodolith beds form the surficial sedimentary layer over millennia-old sediments in the western Menorca  
405 Channel, representing persistent carbon stocks during the Holocene, with with organic carbon averaging  
406 0.57% in the upper 50 cm and showing minimal degradation over ~6,000 years. Although sediment  
407 accretion is slow (median 8.54 cm kyr<sup>-1</sup>), the three-dimensional structure of rhodoliths create a stable  
408 matrix that traps and preserves carbon over millennial timescales, highlighting their role as long-term  
409 reservoirs rather than rapid sinks. These beds have persisted despite human impacts and environmental  
410 changes, actively storing carbon over millennia, and globally, calcified rhodolith deposits are stable over  
411 geological timescales. Given their slow growth and vulnerability to physical disturbance, protection from  
412 trawling or dredging is essential. Conserving rhodolith beds supports biodiversity, ecosystem resilience,  
413 and climate mitigation, emphasizing their often-overlooked contribution to long-term carbon storage.

## 414 **Author contributions**

415 SdJ, FM, and CL conceptualized the study. AC, MdMG, SdJ, RS, and LI conducted sample collection  
416 and processing. MdMG and CL curated the data. SdJ, RS, and AO performed the formal analysis. CL,  
417 RS, and AO developed the methodology. SdJ, FM, and CL prepared the original draft of the manuscript.  
418 HH, JG, and GC contributed to reviewing and editing the manuscript. SdJ, FM, and GC acquired funding.

## 419 **Competing interests**

420 The authors declare that they have no conflict of interest.

## 421 **Acknowledgements**



422 The authors would like to thank the crew of the R/V SOCIB and R/V Sarmiento de Gamboa during the  
423 research cruises, partly funded by the Spanish Ministry of Science and Innovation. We thank the  
424 companies NAUTILUS and GEOMY TSA for their technical support during field work to obtain  
425 geophysical maps and vibrocores.

#### 426 **Financial Support**

427 This work was funded by EU Horizon project MARBEFES (contract no. 101060937) and RHODOMED  
428 (Spanish Ministry of Science grant nº PID2023-146998OB-C22). This work contributes to IMEDEA's  
429 'Center of Excellence' Maria de Maetzu (CEX2021-001198) and ICM's 'Center of Excellence' Severo  
430 Ochoa (CEX2019-000928-5). The Spanish Ministry of Science and Innovation supported S.d.J. with a  
431 "Ramón y Cajal" grant (RyC2020-029062-I), A.O.-A. with a "Ramon y Cajal" grant (RyC2023-043454-  
432 I) and L.I.-L with a FPI predoctoral (PRE2022-104567).

#### 433 **References**

434 Aguirre, J., Braga, J. C., Martín, J. M., and Betzler, C.: Palaeoenvironmental and stratigraphic  
435 significance of Pliocene rhodolith beds and coralline algal bioconstructions from the Carboneras Basin  
436 (SE Spain), *Geodiversitas*, 34, 115–136, 2012.

437 Aguirre, J., Braga, J. C., and Bassi, D.: Rhodoliths and rhodolith beds in the rock record, in:  
438 *Rhodolith/maërl beds: A global perspective*, Springer, 105–138, 2016.

439 Alonso, B., Guillén, J., Canals, M., Serra, J., Acosta, J., Herranz, P., Sanz, J. L., Calafat, A., and  
440 CATAFAU, A.: Los sedimentos de la plataforma continental balear, *Acta Geológica Hispánica*, 185–  
441 196, 1988.

442 Amado-Filho, G. M., Moura, R. L., Bastos, A. C., Salgado, L. T., Sumida, P. Y., Guth, A. Z., Francini-  
443 Filho, R. B., Pereira-Filho, G. H., Abrantes, D. P., Brasileiro, P. S., Bahia, R. G., Leal, R. N., Kaufman,  
444 L., Kleypas, J. a, Farina, M., and Thompson, F. L.: Rhodolith beds are major CaCO<sub>3</sub> bio-factories in  
445 the tropical South West Atlantic., *PloS ONE*, 7, e35171, <https://doi.org/10.1371/journal.pone.0035171>,  
446 2012.

447 Barbier, E. B., Hacker, S. D., Kennedy, C. J., Koch, E. W., Stier, A. C., and Silliman, B. R.: The value  
448 of estuarine and coastal ecosystem services, *Ecological Monographs*, 81, 169–193, 2011.

449 Basso, D.: Deep rhodolith distribution in the Pontian Islands, Italy: a model for the paleoecology of a  
450 temperate sea, *Palaeogeography, palaeoclimatology, palaeoecology*, 137, 173–187, 1998.

451 Basso, D., Caragnano, A., Benzoni, F., Rodondi, G., and others: Southern Sinai rhodoliths: facies,  
452 species composition, and growth rate (Red Sea, Egypt), in: *International rhodolith workshop*, 2012.

453 Basso, D., Babbini, L., Ramos-Esplá, A. A., and Salomidi, M.: Mediterranean rhodolith beds,  
454 *Rhodolith/Maërl Beds: a global perspective*, 281–298, 2017.



- 455 Bernard, G., Romero-Ramirez, A., Tauran, A., Pantalos, M., Deflandre, B., Grall, J., and Grémare, A.:  
456 Declining maerl vitality and habitat complexity across a dredging gradient: insights from in situ  
457 sediment profile imagery (SPI), *Scientific Reports*, 9, 16463, 2019.
- 458 Betzler, C., Braga, J. C., JARAMILLO-VOGEL, D., Roemer, M., Huebscher, C., Schmiedl, G., and  
459 Lindhorst, S.: Late Pleistocene and Holocene cool-water carbonates of the Western Mediterranean Sea,  
460 *Sedimentology*, 58, 643–669, 2011.
- 461 Bianchi, C. N., Morri, C., Chiantore, M., Montefalcone, M., Parravicini, V., Rovere, A., and others:  
462 Mediterranean Sea biodiversity between the legacy from the past and a future of change, *Life in the*  
463 *Mediterranean Sea: a look at habitat changes*, 1, 55, 2012.
- 464 Bracchi, V. A., Caronni, S., Meroni, A. N., Burguett, E. G., Atzori, F., Cadoni, N., Marchese, F., and  
465 Basso, D.: Morphostructural characterization of the heterogeneous rhodolith bed at the marine  
466 protected area “capo carbonara”(Italy) and hydrodynamics, *Diversity*, 14, 51, 2022.
- 467 Cabanellas-Reboredo, M., Mallol, S., Barberá, C., Vergés, A., Díaz, D., and Goñi, R.: Morpho-  
468 demographic traits of two maerl-forming algae in beds with different depths and fishing histories.,  
469 *Aquatic Conservation*, 28, 2018.
- 470 Cabrito, A., de Juan, S., Hinz, H., and Maynou, F.: Morphological insights into the three-dimensional  
471 complexity of rhodolith beds, *Marine Biology*, 171, 127, 2024a.
- 472 Cabrito, A., Maynou, F., Simide, R., Mouillot, D., Lossent, J., and de Juan, S.: Non-extractive fish  
473 diversity assessment in Mediterranean rhodolith beds, *Aquatic Conservation: Marine and Freshwater*  
474 *Ecosystems*, 34, e4212, 2024b.
- 475 Cabrito, A., Maynou, Francesc, de Juan, S., and Peña, V.: Taxonomic complexity and conservation  
476 implications of Mediterranean mesophotic rhodolith beds, *Aquatic Conservation: Marine and*  
477 *Freshwater research*, under review, n.d.
- 478 Canals, M. and Ballesteros, E.: Production of carbonate particles by phytobenthic communities on the  
479 Mallorca-Menorca shelf, northwestern Mediterranean Sea, *Deep Sea Research Part II: Topical Studies*  
480 *in Oceanography*, 44, 611–629, 1997.
- 481 Ehrhold, A., Jouet, G., Le Roy, P., Jorry, S. J., Grall, J., Reixach, T., Lambert, C., Gregoire, G., Goslin,  
482 J., Roubi, A., and others: Fossil maerl beds as coastal indicators of late Holocene palaeo-environmental  
483 evolution in the Bay of Brest (Western France), *Palaeogeography, Palaeoclimatology, Palaeoecology*,  
484 577, 110525, 2021.
- 485 Fornós, J. J. and Ahr, W.: Temperate carbonates on a modern, low-energy, isolated ramp; the Balearic  
486 platform, Spain, *Journal of Sedimentary Research*, 67, 364–373, 1997.
- 487 Guillén, J.: La sedimentación carbonatada en la plataforma continental de Campos (Sur de Mallorca),  
488 1987.
- 489 Howard, J. L., Creed, J. C., Aguiar, M. V., and Fourqurean, J. W.: CO<sub>2</sub> released by carbonate sediment  
490 production in some coastal areas may offset the benefits of seagrass “Blue Carbon” storage, *Limnology*  
491 *and Oceanography*, 63, 160–172, 2018.



- 492 Illa-López, L., Cabrito, A., de Juan, S., Maynou, F., and Demestre, M.: Distribution of rhodolith beds  
493 and their functional biodiversity characterisation using ROV images in the western Mediterranean Sea,  
494 *Science of the Total Environment*, 905, 167270, 2023.
- 495 Jardim, V. L., Grall, J., Barros-Barreto, M. B., Bizien, A., Benoit, T., Braga, J. C., Brodie, J., Burel, T.,  
496 Cabrito, A., Diaz-Pulido, G., and others: A common terminology to unify research and conservation of  
497 coralline algae and the habitats they create, *Aquatic Conservation: Marine and Freshwater Ecosystems*,  
498 35, e70121, 2025.
- 499 Joher, S., Ballesteros, E., and Rodríguez-Prieto, C.: Macroalgal-dominated coastal detritic communities  
500 from the Western Mediterranean and the Northeastern Atlantic, *Mediterranean Marine Science*, 17,  
501 476–495, 2016.
- 502 de Juan, S., Lo Iacono, C., and Demestre, M.: Benthic habitat characterisation of soft-bottom  
503 continental shelves: Integration of acoustic surveys, benthic samples and trawling disturbance intensity,  
504 *Estuarine, Coastal and Shelf Science*, 117, 199–209, <https://doi.org/10.1016/j.ecss.2012.11.012>, 2013.
- 505 de Juan, S., Ospina-Alvarez, A., Hinz, H., Moranta, J., and Barberá, C.: The continental shelf seascape:  
506 a network of species and habitats, *Biodiversity and Conservation*, 1–20, 2023.
- 507 Keil, R. G., Tsamakis, E., Fuh, C. B., Giddings, J. C., and Hedges, J. I.: Mineralogical and textural  
508 controls on the organic composition of coastal marine sediments: Hydrodynamic separation using  
509 SPLITT-fractionation, *Geochimica et Cosmochimica Acta*, 58, 879–893, 1994.
- 510 Lambeck, K.: Late Pleistocene and Holocene sea-level change in Greece and south-western Turkey: a  
511 separation of eustatic, isostatic and tectonic contributions, *Geophysical Journal International*, 122,  
512 1022–1044, 1995.
- 513 Lambeck, K. and Bard, E.: Sea-level change along the French Mediterranean coast for the past 30 000  
514 years, *Earth and Planetary Science Letters*, 175, 203–222, 2000.
- 515 Lo Iacono, C., Mateo, M. A., Gracia, E., Guasch, L., Carbonell, R., Serrano, L., Serrano, O., and  
516 Danobeitia, J.: Very high-resolution seismo-acoustic imaging of seagrass meadows (Mediterranean  
517 Sea): Implications for carbon sink estimates, *Geophysical Research Letters*, 35, 2008.
- 518 de Macêdo Carneiro, P. B., de Lima, J. P., Bandeira, Ê. V. P., Neto, A. R. X., Barreira, C. de A. R., de  
519 Souza Tâmega, F. T., Matthews-Cascon, H., Junior, W. F., and de Morais, J. O.: Structure, growth and  
520 CaCO<sub>3</sub> production in a shallow rhodolith bed from a highly energetic siliciclastic-carbonate coast in  
521 the equatorial SW Atlantic Ocean, *Marine environmental research*, 166, 105280, 2021.
- 522 Macreadie, P. I., Anton, A., Raven, J. A., Beaumont, N., Connolly, R. M., Friess, D. A., Kelleway, J. J.,  
523 Kennedy, H., Kuwae, T., Lavery, P. S., and others: The future of Blue Carbon science, *Nature*  
524 *communications*, 10, 3998, 2019.
- 525 Mao, J., Burdett, H. L., McGill, R. A., Newton, J., Gulliver, P., and Kamenos, N. A.: Carbon burial over  
526 the last four millennia is regulated by both climatic and land use change, *Global Change Biology*, 26,  
527 2496–2504, 2020.
- 528 Middelburg, J. J.: Reviews and syntheses: to the bottom of carbon processing at the seafloor,  
529 *Biogeosciences*, 15, 413–427, 2018.



- 530 Moranta, J., Barberá, C., Druet, M., and Zaragoza, N.: Caracterización ecológica de la plataforma  
531 continental (50-100 m) del canal de Menorca. Informe final área LIFE+ INDEMARES  
532 (LIFE07/NAT/E/000732), Instituto Español de Oceanografía-Centro Oceanográfico de Baleares  
533 (Palma), 2014.
- 534 Nellemann, C. and Corcoran, E.: Blue carbon: the role of healthy oceans in binding carbon: a rapid  
535 response assessment, UNEP/Earthprint, 2009.
- 536 Olmstead, S. A. and Andrus, C. F. T.: Growth characterization of mesophotic rhodoliths in the northern  
537 Gulf of Mexico using radiocarbon dating, *Palaeogeography, Palaeoclimatology, Palaeoecology*, 654,  
538 112438, 2024.
- 539 Rendina, F., Kaleb, S., Caragnano, A., Ferrigno, F., Appolloni, L., Donnarumma, L., Russo, G. F.,  
540 Sandulli, R., Roviello, V., and Falace, A.: Distribution and characterization of deep rhodolith beds off  
541 the Campania coast (SW Italy, Mediterranean Sea), *Plants*, 9, 985, 2020.
- 542 Riosmena-Rodríguez, R., Nelson, W., and Aguirre, J.: Rhodolith/maërl beds: a global perspective,  
543 Springer, 2017.
- 544 Schubert, N., Tuya, F., Peña, V., Horta, P. A., Salazar, V. W., Neves, P., Ribeiro, C., Otero-Ferrer, F.,  
545 Espino, F., Schoenrock, K., and others: “Pink power”—the importance of coralline algal beds in the  
546 oceanic carbon cycle, *Nature Communications*, 15, 8282, 2024.
- 547 Tabone, L., Knittweis, L., Aguilar, R., Alvarez, H., Borg, J. A., Garcia, S., Schembri, P. J., and Evans,  
548 J.: Habitat characterization, anthropogenic impacts and conservation of rhodolith beds off southeastern  
549 Malta, *Aquatic Conservation: Marine and Freshwater Ecosystems*, 34, e4148, 2024.
- 550 Tauran, A., Dubreuil, J., Guyonnet, B., and Grall, J.: Impact of fishing gears and fishing intensities on  
551 maerl beds: An experimental approach, *Journal of Experimental Marine Biology and Ecology*, 533,  
552 151472, 2020.
- 553 Teichert, S.: Attached and free-living crustose coralline algae and their functional traits in the  
554 geological record and today, *Facies*, 70, 8, 2024.
- 555 Trégarot, E., D’Olivo, J. P., Botelho, A. Z., Cabrito, A., Cardoso, G. O., Casal, G., Cornet, C. C., Cragg,  
556 S. M., Degia, A. K., Fredriksen, S., and others: Effects of climate change on marine coastal  
557 ecosystems—A review to guide research and management, *Biological Conservation*, 289, 110394, 2024.
- 558 Tuya, F., Schubert, N., Aguirre, J., Basso, D., Bastos, E. O., Berchez, F., Bernardino, A. F., Bosch, N.  
559 E., Burdett, H. L., Espino, F., and others: Levelling-up rhodolith-bed science to address global-scale  
560 conservation challenges, *Science of The Total Environment*, 164818, 2023.
- 561 Van der Heijden, L. and Kamenos, N.: Calculating the global contribution of coralline algae to carbon  
562 burial, *Biogeosciences*, 12, 7845–7877, 2015.
- 563
- 564
- 565